Studies on the Mechanism by Which the Formation of Nanocomposites Enhances Thermal Stability†

Jin Zhu,‡ Fawn M. Uhl,‡ Alexander B. Morgan,§,⊥ and Charles A. Wilkie*,‡

Department of Chemistry, Marquette University, P.O. Box 1881, Milwaukee, Wisconsin 53201, and Fire Science Division, Building and Fire Research Laboratory, National Institute of Standards and Technology, Gaithersburg, Maryland 20899

Received May 7, 2001. Revised Manuscript Received August 29, 2001

Polystyrene−clay and polystyrene−graphite nanocomposites have been prepared and used to explore the process by which the presence of clay or graphite in a nanocomposite enhances the thermal stability of polymers. This study has been designed to determine if the presence of paramagnetic iron in the matrix can result in radical trapping and thus enhance thermal stability. Nanocomposites were prepared by bulk polymerization using both iron-containing and iron-depleted clays and graphites, and they were characterized by X-ray diffraction, transmission electron microscopy, thermogravimetric analysis, and cone calorimetry. The presence of structural iron, rather than that present as an impurity, significantly increases the onset temperature of thermal degradation in polymer−clay nanocomposites. Intercalated nanocomposites show an iron effect, but this is less important for exfoliated systems. Polymer−graphite nanocomposites show no difference between iron-free and iron-containing nanocomposites, presumably because the iron is not nanodispersed in the graphite.

Introduction

Many reports have appeared on the enhanced mechanical properties of polymer−clay nanocomposites relative to the virgin polymer or to systems in which the clay is not dispersed at the nano level.[1,2,3] (Reference 2 contains a wealth of data to which the interested reader is referred.) There have been a smaller, yet substantial, number of papers that show that these nanocomposites show higher thermal stability and a reduced rate of heat release in the cone calorimeter.[4−9] The mechanism by which this is accomplished is not clear. Only one suggested mechanism has been published, and that suggests that the barrier properties of the nanocomposite are responsible for this enhancement.[9] Barrier properties could include both the thermal barrier, which protects the polymer from fire, and the mass transport barrier, which makes it difficult for degradation products to leave the polymer. Recent molecular dynamics simulations of the thermal degradation of nanoconfined polypropylene support this mechanistic hypothesis.[10] Recent work from this laboratory on polystyrene−graphite nanocomposites has shown that there is some enhanced stabilization but that it is not as great as seen with clay nanocomposites.[11]

Recent work from this laboratory[6] has shown that even when the fraction of clay was as low as 0.1%, the peak heat release rate in a cone calorimeter is lowered by 40%, a value not much different from that observed at higher amounts of clay. In a separate investigation, it was found that the reduction in peak heat release at 1% clay is 64% of that at 3 or 5% clay.[7] In other words, at very low clay level there is still some significant effect on the rate of heat release and it seems unlikely that enough of a barrier could be formed at this low loading of clay to lead to these enhanced thermal properties.

As a result of these observations, we wondered if iron or other paramagnetic sites within the clay could function as radical traps to at least partially prevent degradation. In this study, polystyrene nanocomposites have been prepared in which more or less identical clays, some of which contain iron and some which do not, are ion-exchanged with the same ammonium ions so that clearly comparable nanocomposites are prepared and characterized. An analogous study has been carried out comparing purified graphites and those which contain iron.

Experimental Section

Materials. The synthetic clay Barasym SSM-100 was provided by the Clay Mineral Repository at the University of

* To whom correspondence should be addressed.

† It is the policy of the National Institute of Standards and Technology to use the International System of Units (metric units) in its technical communications. However in this document other units are used to conform to the publisher's style.

‡ Marquette University.

§ National Institute of Standards and Technology.

⊥ Current Address: The Dow Chemical Company, Nanomaterials Group, Midland, MI 48674.

(1) Pinnavaia, T. J. *Science* **1983**, 220, 365−371.

(2) Alexandre M.; Dubois, P. *Mater. Sci. Eng.* **2000**, *R28*, 1−63.

(3) Kojima, Y.; Usuki, A.; Kawasumi, M.; Okada, A.; Fukushima, Y.; Karauchi, T.; Kamigaito, O. *J. Mater. Res.* **1993**, 7, 185.

(4) Gilman, J. W.; Kashiwagi, T.; Giannelis, E. P.; Manias, E.; Lomakin, S.; Lichtenham, J. D.; Jones. P. In *Fire Retardancy of Polymers: The Use of Intumescence*; Le Bras, M., Camino, G., Bourbigot, S., Delobel, R., Eds.; Royal Society of Chemistry: London, 1998; pp 201−221.

(5) Gilman, J. W.; Kashiwagi, T.; Nyden, M.; Brown, J. E. T.; Jackson, C. L.; Lomakin, S.; Gianelis, E. P.; Manias, E. In *Chemistry and Technology of Polymer Additives*; Al-Malaika, S., Golovoy, A., Wilkie, C. A., Eds.; Blackwell Scientific, 1999; pp 249−265.

(6) Zhu, J.; Wilkie C. A. *Polym. Int.* **2000**, *49*, 1158−1163.

(7) Zhu, J.; Morgan, A. B.; Lamelas, F. J.; Wilkie, C. A. *Chem. Mater.*, in press.

(8) Doh, J. D.; Cho, I. *Polym. Bull.* **1998**, *41*, 511−518.

(9) Gilman, J. W.; Kashiagi, T. In *Polymer−Clay Nanocomposites*; Pinnavaia, T. J., Beall, G. W., Eds.; John Wiley & Sons: New York, 2000; pp 193−206.

(10) Nyden, M. R.; Gilman, J. W. *Comp. and Theo. Polym. Sci.* **1997**, *7*, 191−198.

(11) Uhl, F. M.; Wilkie, C. A., submitted for publication.

10.1021/cm010451y CCC: $20.00
Published on Web 11/01/2001

Missouri−Columbia. This clay is a synthetic mica−montmorillonite (SMM), which has structure similar to montmorillonite (MMT). The reported elemental composition is as follows (%): SiO_2, 49.7; Al_2O_3, 38.2; TiO_2, 0.023; Fe_2O_3, 0.02; MgO, 0.014; Na_2O, 0.26; K_2O, <0.01; Li_2O, 0.25; F, 0.76; P_2O_5, 0.001; S, 0.10. The cation-exchange capacity (CEC) is 140 mequiv/100 g, and the cation in the gallery space is ammonium. The sodium−montmorillonite clay was provided by Southern Clay Products, Inc.; the elemental composition is as follows (%): SiO_2, 57.7; Al_2O_3, 19.0; TiO_2, 0.12; Fe_2O_3, 4.2; MgO, 2.14; Na_2O, 4.0; K_2O, 0.08; P_2O_5, 0.02. The cation exchange capacity is 92 mequiv/100 g MMT, and the counterion is sodium. Two additional montmorillonite clays were provided by Nanocor, Inc., PGW and S−PGW. These clays are identical except that one of them, S−PGW, has had iron magnetically removed. The iron that remains in S−PGW is structural iron. One should note that only 0.06% of the iron has been removed by this process; the majority of the iron impurity is substituted for either silicon or aluminum in the clay. The composition of PGW is as follows (%): SiO_2, 50.9; Al_2O_3, 19.24; TiO_2, 0.24; Fe_2O_3, 3.06; MgO, 2.56; Na_2O, 3.6; K_2O, 0.08; P_2O_5, 0.01; CaO, 0.16; SO_3, 0.14. The composition of S−PGW is as follows (%): SiO_2, 51.7; Al_2O_3, 20.0; TiO_2, 0.04; Fe_2O_3, 3.00; MgO, 2.5, Na_2O; 3.8; K_2O, 0.07; P_2O_5, 0.01; CaO, 0.17; SO_3, 0.24. Graphites were kindly provided by Asbury Graphite Mills; one was a powder of 1−2 μmsize and contained no iron. Two iron-containing graphites were used; one was amorphous, 20 μm in size (G505), while the other was a flake of 40 μm size (9092). The iron is inhomogeneously distributed in the graphite; levels range from 3 to 14% as Fe_2O_3.

The majority of chemicals used in this study, including styrene, stearyltributylphosphonium bromide, P18, 2,2′-azobis-(isobutyronitrile) (AIBN), vinylbenzyl chloride, ethyl acetate, and inhibitor removal columns, were purchased from Aldrich Chemical Co. Hydrogenated tallow dimethylbenzylammonium chloride (M2HTB) was provided by Akzo Nobel. TCI America supplied *N*,*N*-dimethyl-*n*-hexadecylamine. *N*,*N*-dimethyl-*n*-hexdecyl-(*p*-vinylbenzyl)ammonium chloride (VB16) has been previously used in these laboratories, and its preparation has been described.[7]

Instrumention. IR spectroscopy, FTIR, was performed on a Mattson Galaxy IR spectrometer at 4 cm^{-1} resolution. Thermogravimetric analysis, TGA, was performed on an Omnitherm1000 unit under either a flowing nitrogen or an air atmosphere at a scan rate of 10 °C per minute from 20 to 600 °C. TGA/FTIR were carried out using a Cahn model 131 balance interfaced to a Mattson Galaxy IR spectrometer under a nitrogen atmosphere at a flow rate of 40 cm^3 min^{-1}. All TGA experiments have been performed at least two times, and some have been done in triplicate. Reproducibility of temperatures is ±2 °C, while the amount of nonvolatile residue is reproducible to ±2%. Cone calorimetry at 35 kW m^{-2} was performed using a Stanton-Redcroft/PL Thermal Sciences instrument according ASTM E 1354-92 at an incident flux of 35 kW m^{-2} using a cone-shaped heater. Exhaust flow was set at 24 L s^{-1}, and the spark was continuous until the sample ignited. The results at 50 kW m^{-2} were obtained on an Atlas CONE-2. Cone samples were prepared by compression, molding the samples (20−50 g) into square plaques using a heated press. All samples were run in duplicate, and the average value is reported; typical results from cone calorimetry are reproducible to within about ±10%.[5] X-ray diffraction (XRD) measurements were performed using a Rigaku powder diffractometer, with a Cu tube source (λ = 1.54 Å) operated at 1 kW. Scans were taken from 2θ = 0.70−30, step size = 0.11, and a scan time per step of 20 s using the high-resolution mode. Bright field transmission electron microscopy (TEM) images of the composites were obtained at 120 kV, at low-dose conditions, with a Phillips 400T electron microscope. The samples were ultramicrotomed with a diamond knife on a Leica Ultracut UCT microtome at room temperature to give 70 nm thick sections. The sections were transferred from water to carbon-coated Cu grids of 200 mesh. The contrast between the layered silicates and the polymer phase was sufficient for imaging, so no heavy metal staining of sections prior to imaging was required.

VB16 and the corresponding polystyrene−clay nanocomposites were prepared following a procedure previously reported.[6,7] Nanocomposites were prepared using VB16, M2HTB, stearyltributylphosphonium bromide, and P18, for the four clays, SMM, MMT, PGW, and S−PGW, mentioned above; i.e., the following nanocomposites were prepared: PS−SMM−VB16, PS−SMM−M2HTB, PS−SMM−P18, PS−MMT−VB16, PS−MMT−M2HTB, PS−MMT−P18, PS−PGW−VB16, and PS−S−PGW−VB16. Standard terminology is to add the percentage of clay following the descriptor; i.e., PS−MMT−VB16-3 contains 3% clay. The polystyrene−graphite nanocomposites were prepared as previously described[11] using potassium graphite, KC_8, as the initiator.

Results and Disscussion

Polystyrene−Clay Nanocomposites. Two organic ammonium cations and a phosphonium cation were used in this study. One of these, VB16, gives an exfoliated structure for MMT, while M2HTB gives an intercalated structure, and an analagous phosphonium cation (hexadecyltriphenylphosphonium) gives a mixture of intercalated and exfoliated structures.[6,7] The structures of the salts that were used for the preparation of the organically modified clays are shown below. By a comparison of these systems, any effects due to intercalation vs exfoliation can be understood. The clays were chosen to have the most similarity between the iron-containing and the iron-depleted nanocomposites. It has been shown that the thermal degradation of the clays, actually it is the cation which degrades, proceeds via a Hofmann elimination, i.e., the loss of an olefin from the cation, followed by the loss of the amine or phosphine to give only a proton occupying the cationic site.[7,12] The degradation of the organically modified synthetic clay, SMM-VB16, has been studied by TGA/FTIR techniques, and the course of the degradation is identical to that observed for MMT−VB16.[7] The degradation begins at about 200 °C with the loss of the olefin, and its evolution continues to 400 °C. Above this temperature, IR bands typical of the amine are observed. The evolution of volatiles agrees within 2% to the fraction of ammonium salt contained within the clay.

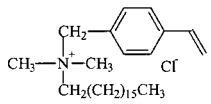

VB16

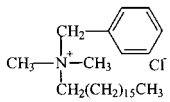

M2HTB

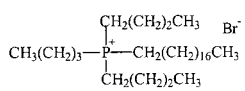

P18

Characterization of Nanocomposites by XRD and TEM. Characterization of a nanocomposite requires the measurement by both XRD and TEM. XRD

(12) Xie, W.; Gao, Z.; Pan, W. P.; Vaia, R.; Hunter, D.; Singh, A. *Polym. Mater. Sci. Eng.* **2000**, *83*, 284.

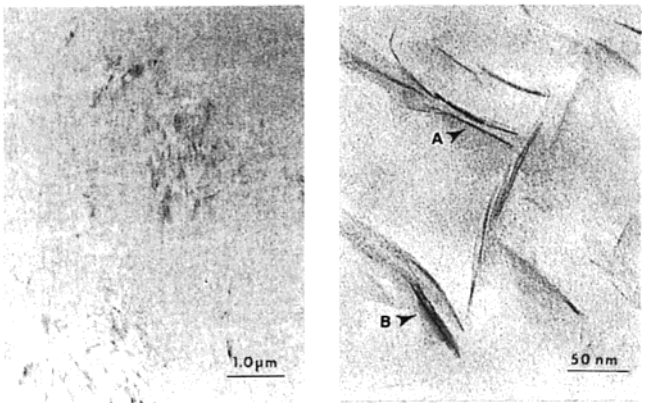

Figure 1. TEM images of the polystyrene nanocomposite of synthetic montmorillonite, SMM, derivatized with VB16.

Table 1. XRD Data for Clays and PS−Nanocomposites from Those Clays

clays	d_{001} of clay, nm	d_{001} of nanocomposite, nm
Na−MMT	1.20	
MMT−VB16	2.87	not observed
MMT−M2HTB	1.91	3.40
MMT−P18	2.32	2.83
NH_4−SMM	1.09	
SMM−VB16	4.53	not observed
SMM−M2HTB	5.04	5.88
SMM−P18	4.83	5.95
Na−S−PGW	1.21	
S−PGW−M2HTB	2.95	3.40
Na−PGW	1.23	
PGW−M2HTB	2.76	3.55

gives the d spacing of clay while TEM shows the actual dispersion, at both micro and nanoscale, of the system.

The XRD data for all of the nanocomposites described herein and the clays from which they were produced are shown in Table 1. Two things are noteworthy in this table; (1) the absence of a peak for the VB16 nanocomposites, which is perhaps indicative of an exfoliated structure, and (2) the very large d spacing for the synthetic clays, SMM. Since the d spacing increases in all cases, the formation of some nanocomposite, rather than an immiscible system, is indicated.

The TEM images of the PS−SMM−VB16 and the PS−SMM−M2HTB nanocomposites are shown in Figures 1 and 2, respectively. There is a difference between these; the VB16 material is partially exfoliated while the M2HTB is intercalated. This is an identical result

Table 2. TGA Data, in Nitrogen, for SMM and MMT Polystyrene Nanocomposites

nanocomposite	clay concn	$T_{0.1}$, °C (diff)[a]	$T_{0.5}$, °C (diff)[a]	char at 600 °C, % (diff)[a]
PS		351	404	0
PS−SMM−VB16	0.1	340	378	1
PS−SMM−VB16	0.5	339	383	4
PS−SMM−VB16	1	378	428	3
PS−SMM−VB16	3	401	441	9
PS−SMM−VB16	5	392	439	8
PS−MMT−VB16	0.1	402 (62)	429 (51)	1 (0)
PS−MMT−VB16	0.5	397 (58)	434 (51)	2 (−2)
PS−MMT−VB16	1	405 (27)	438 (10)	3 (0)
PS−MMT−VB16	3	408 (7)	444 (3)	6 (−3)
PS−MMT−VB16	5	417 (25)	448 (9)	6 (−2)
PS−SMM−M2HTB	0.1	358	407	1
PS−SMM−M2HTB	0.5	346	391	4
PS−SMM−M2HTB	1	377	429	5
PS−SMM−M2HTB	3	364	434	4
PS−SMM−M2HTB	5	372	436	8
PS−MMT−M2HTB	0.1	395 (37)	425 (18)	1 (0)
PS−MMT−M2HTB	0.5	399 (53)	433 (42)	2 (−2)
PS−MMT−M2HTB	1	399 (22)	435 (7)	4 (−1)
PS−MMT−M2HTB	3	396 (32)	435 (1)	4 (0)
PS−MMT−M2HTB	5	398 (26)	445 (9)	5 (−3)
PS−MMT−P18	3	361	420	4
PS−MMT−P18	3	396 (35)	425 (5)	4 (0)

[a] Diff = $T_{\text{iron-containing}} - T_{\text{iron-free}}$ and $\text{diff}_{\text{char}} = \text{char}_{\text{iron-containing}} - \text{char}_{\text{iron-free}}$.

Table 3. TGA Data, in Nitrogen, for PGW and S−PGW Polystyrene Nanocomposites

nanocomposite	clay concn	$T_{0.1}$, °C (diff)[a]	$T_{0.5}$, °C (diff)[a]	char at 600 °C, % (diff)[a]
PS		351	404	0
PS−SPGW−M2HTB	0.1	396	433	1
PS−SPGW−M2HTB	0.5	401	441	1
PS−SPGW−M2HTB	1	396	442	1
PS−SPGW−M2HTB	3	400	447	3
PS−SPGW−M2HTB	5	400	452	4
PS−PGW−M2HTB	0.1	402 (6)	440 (7)	1 (0)
PS−PGW−M2HTB	0.5	403 (2)	441 (0)	1 (0)
PS−PGW−M2HTB	1	408 (11)	454 (12)	1 (0)
PS−PGW−M2HTB	3	415 (15)	456 (9)	4 (1)
PS−PGW−M2HTB	5	422 (22)	463 (11)	5 (1)

[a] Diff = $T_{\text{iron-containing}} - T_{\text{iron-free}}$ and $\text{diff}_{\text{char}} = \text{char}_{\text{iron-containing}} - \text{char}_{\text{iron-free}}$.

which has been previously observed for the MMT nanocomposites.[6,7] In the case of the VB16-containing nanocomposite, polymerization of styrene may occur onto the cation, while this is not possible with the M2HTB system. One may conclude that the possibility of polymerization onto the cation may promote, at least with styrenic systems, the possibility of exfoliation.

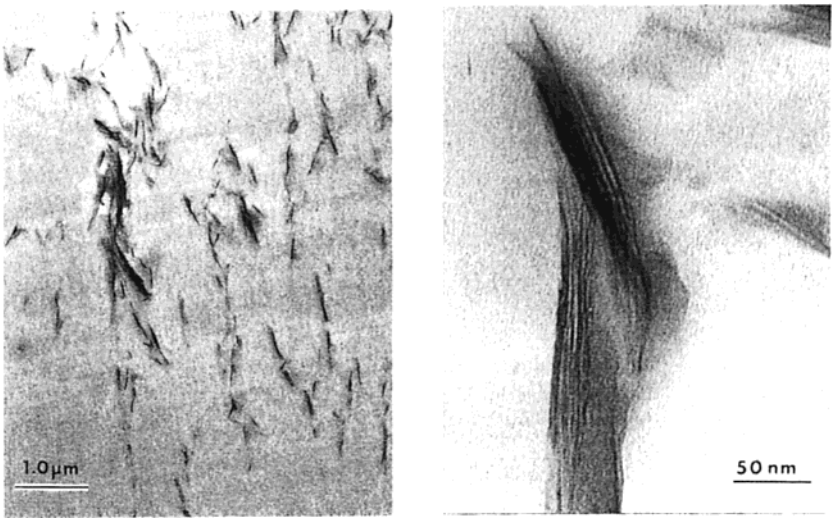

Figure 2. TEM images of the polystyrene nanocomposite of synthetic montmorillonite, SMM, derivatized with M2HTB.

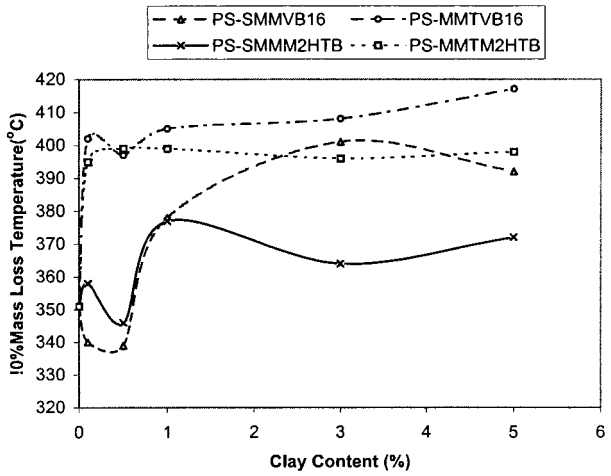

Figure 3. The 10% mass loss temperature of M2HTB and VB16 nanocomposites.

Table 4. TGA Results, in Air, for Iron-Containing and Iron-Free Polystyrene Nanocomposites

nanocomposite	$T_{0.1}$, °C	$T_{0.5}$, °C	char at 600 °C, %
PS−MMT−M2HTB-3	318	387	4
PS−SMM−M2HTB-3	312	391	4
PS−MMT−VB16-3	342	401	5
PS−SMM−VB16-3	328	394	6
PS−PGW-3	316	383	3
PS−SPGW-3	320	387	5

TGA Characterization of Thermal Stability of the Nanocomposites. The TGA data for the SMM and MMT nanocomposites, in nitrogen, as a function of the amount of clay is shown in Table 2, and that for the PGW and S−PGW nanocomposites is shown in Table 3; P18 has only been examined at 3% clay and only for MMT and SMM. The data shows the temperatures at which 10% degradation occurs, $T_{0.1}$, as a measure of the onset of the degradation, and at which 50% degradation occurs, $T_{0.5}$, as the midpoint of the degradation process, and the fraction that is nonvolatile at 600 °C, identified as char. In addition, the difference between the iron-containing and the iron-free clay is also recorded.

The onset temperatures as well as the midpoint of the degradation are clearly lower for the iron-containing MMT than for the iron-free SMM. One might expect that the barrier properties would be lowest at low amounts of clay and expect to see a greater difference between the iron-containing and the iron-free clays at low clay amounts. For the VB16 (exfoliated) system, there is a 62 °C difference for the 0.1% clay sample and a 58 °C difference for the 0.5% clay sample but the differences are half this value, or less, as the fraction of clay increases. The difference in the temperatures at which 10% degradation occurs for MMT vs SMM is shown in Figure 3. The amount of nonvolatile residue which remains at the end of a TGA run shows no change with or without the presence of iron. Thus, the presence of iron does not lead to enhanced char formation but it does affect the onset of the degradation.

The differences for the PGW−SPGW family of clays is much smaller than that observed for MMT−SMM. While SMM contains essentially no iron, only nonstructural iron has been removed in the PGW−SPGW pair. On the basis of the TGA results, it appears that structural iron, and not paramagnetic impurities, is the effective agent by which radical trapping occurs.

TGA Measurements in Air. To ascertain the role that air may play in this degradation, TGA measurements on the nanocomposites, which contain 3% clay, have also been performed in air; the results are shown in Table 4. The effect of iron is much reduced in air for the M2HTB system, a difference of 32 °C in nitrogen but only 6 °C in air. However, for the VB16 system, one observes a 7 °C difference in nitrogen but a 14 °C difference in air. Thermal degradation in air invariably occurs at a lower temperature than in nitrogen. It is commonly felt that TGA measurements in nitrogen are of the most value for fire retardancy, because it is believed that the thermal degradation of the surface

Table 5. Cone Calorimetry for SMM−MMT Nanocomposites at 35 kW m^{-2}

nanocomposite	$t_{ignition}$[a] (s)	PHRR,[a] (kW m^{-2}) (% diff)[b]	t_{PHRR} (s)	mean HRR [a] (kW m^{-2})	ASEA[a] (m^2 kg^{-1})	AMLR[a] (g(sm)$^{-2}$)
PS	35	1024	165	479	1713	0.13
PS−SMM−VB16-0.1	35	758	180	437	1530	0.15
PS−SMM−VB16-0.5	20	807	175	433	1359	0.13
PS−SMM−VB16-1	33	785	180	470	1484	0.14
PS−SMM−VB16-3	32	597	210	431	1591	0.12
PS−SMM−VB16-5	24	444	240	348	1666	0.10
PS−MMT−VB16-0.1	20	890 (−17)	153	439	1270	0.13
PS−MMT−VB16-0.5	20	771 (4)	140	407	1338	0.11
PS−MMT−VB16-1	20	752 (4)	165	401	1330	0.12
PS−MMT−VB16-3	10	584 (2)	185	405	1430	0.11
PS−MMT−VB16-5	35	534 (−20)	180	390	1461	0.09
PS−SMM−P18-3	15	556	150	366	1127	0.12
PS−MMT−P18-3	25	566 (−2)	165	411	1252	0.12
PS−SMM−M2HTB-0.1	20	793	185	436	1248	0.12
PS−SMM−M2HTB-0.5	17	814	168	440	1494	0.14
PS−SMM−M2HTB-1	15	806	185	473	1295	0.13
PS−SMM−M2HTB-3	20	642	205	421	1571	0.13
PS−SMM−M2HTB-5	20	517	227	385	1659	0.10
PS−MMT−M2HTB-0.1	40	593 (25)	165	322	1202	0.11
PS−MMT−M2HTB-0.5	40	697 (14)	190	392	1097	0.12
PS−MMT−M2HTB-1	50	663 (18)	175	376	992	0.11
PS−MMT−M2HTB-3	20	449 (30)	170	321	1448	0.10
PS−MMT−M2HTB-5	45	412 (20)	230	307	1271	0.09

[a] $t_{ignition}$, time to ignition; PHRR, peak heat release rate; t_{PHRR}, time to peak heat release rate; mean HRR, mean heat release rate; ASEA, average specific extinction area; (smoke production) AMLR, average mass loss rate. [b] %diff = [PHRR(no iron) − PHRR(iron)/PHRR (no iron)] × 100.

Table 6. Cone Calorimetry for the PGW−SPGW Nanocomposites at 50 kW m^{-2}

nanocomposite	$t_{ignition}$[a] (s)	PHRR[a] (kW m^{-2}) (% diff)[b]	t_{PHRR}[a] (s)	mean HRR[a] (kW m^{-2})	ASEA[a] (m^2 kg^{-1})	AMLR[a] (g(sm)$^{-2}$)
PS	42	1845	118	946	1265	35
PS−S−PGW−M2HTB-0.1	41	1395	121	752	1421	32
PS−S−PGW−M2HTB-0.5	42	1318	133	644	1450	31
PS−S−PGW−M2HTB-1	33	1170	121	603	1520	25
PS−S−PGW−M2HTB-3	34	825	145	498	1645	20
PS−S−PGW−M2HTB-5	35	799	124	529	1677	20
PS−PGW−M2HTB-0.1	46	1260 (10)	118	691	1370	32
PS−PGW−M2HTB-0.5	45	1195 (9)	133	654	1402	31
PS−PGW−M2HTB-1	24	1034 (12)	115	570	1409	26
PS−PGW−M2HTB-3	19	858 (4)	100	510	1578	22
PS−PGW−M2HTB-5	16	775 (3)	94	442	1606	19

[a] $t_{ignition}$, time to ignition; PHRR, peak heat release rate; t_{PHRR}, time to peak heat release rate; mean HRR, mean heat release rate; ASEA, average specific extinction area; (smoke production) AMLR, average mass loss rate. [b] %diff = [PHRR(no iron) − PHRR(iron)/ PHRR (no iron)] × 100.

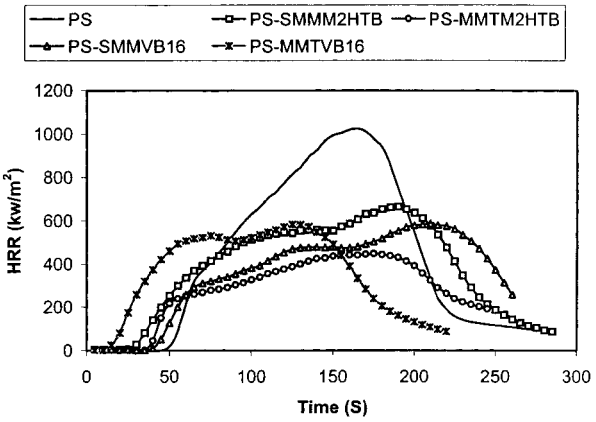

Figure 4. Heat release rate of M2HTB and VB16 clay nanocomposites as a function of time in seconds.

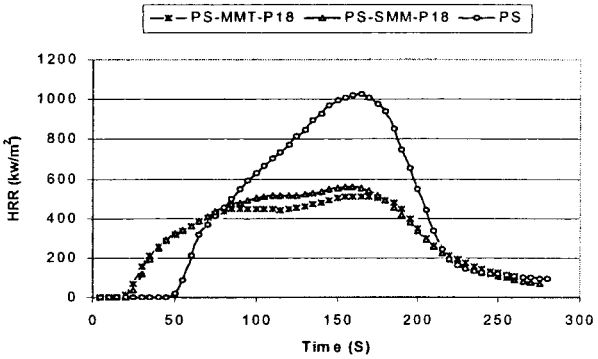

Figure 5. Heat release rate of PS−P18 nanocomposites.

layer of a polymer in the presence of a heat source occurs in a reducing, and not an oxidizing, environment.[13]

Cone Calorimetric Characterization of the Nanocomposites. All of the cone calorimetric data for the polystyrene−clay nanocomposites is shown in Tables 5 and 6.

The difference in peak heat release rate, PHRR, for the iron-containing clay, MMT, and the iron-free clay, SMM, is consistently larger for the M2HTB salts but never exceeds experimental error for VB16 and P18. Plots of PHRR for the VB16 and M2HTB systems are shown in Figure 4 while data for P18 is in Figure 5.

Gilman et al. have previously suggested that intercalated nanocomposites may show enhanced thermal stability relative to the exfoliated materials.[14] Since there is a much greater effect from the presence of iron with the M2HTB nanocomposite, which is known to be intercalated, than from the exfoliated VB16 nanocomposite and the exfoliated/intercalated P18, it is possible that the presence of iron does lead to some radical trapping which enhances thermal stability, and this is more important for intercalated than for exfoliated nanocomposites.

For the PGW and S−PGW set, the PHRRs are within experimental error throughout the entire range of concentration; there is no difference between these materials in the cone calorimeter. The difference in iron content is small (3.06 vs 3.00%), and the supplier states that the paramagnetic iron has been removed and all that remains is iron which is integral to the structure of the clay. The percentage decrease in PHRR, compared to virgin polymer, is actually greater for this system than for the SMM−MMT pair, but the removal of paramagnetic impurities does not seem to effect the PHRR. We, therefore, assume that structural iron must be the important site of radical trapping.

Iron may be present in the clay either as an impurity or as a substitute for the aluminum or silicon atoms which comprise the structure of the aluminosilicate material. When iron is present as an impurity, it cannot be well-dispersed but must be clustered in particular regions of the structure and thus it cannot be effective as a radical trap. On the other hand, if the iron is substituted within the clay structure, it must be nanodispersed within the polymer and thus can be available throughout the material.

The time to ignition of the nanocomposites is actually lower than that of virgin polystyrene. This has been observed with other nanocomposites and correlates with the observation that nanocomposites will usually burn. If one hopes to use nanocomposite technology to enhance the fire retardancy of polymers, one will probably need to combine the clay with a conventional vapor-phase fire retardant to provide the extinguishability which is required.

Polystyrene−Graphite Nanocomposites. The d spacing in graphite is 3.35 Å, expanding to 5.41 Å in KC_8 and to 15−22 Å in the polystyrene nanocomposites.

(13) Lyon, R. E. In *Fire Retardancy of Polymeric Materials*; Grand, A. F., Wilkie, C. A., Eds.; Marcel Dekker: New York, 2000; p 392.

(14) Gilman, J. W.; Kashiwagi, T. In *Polymer-Clay Nanocomposites*; Pinnavaia, T. J., Beall, G. W., Eds.; John Wiley & Sons: New York, 2000; pp 193−205.

Table 7. Thermogravimetric Analysis, in Nitrogen, of Graphite−Polystyrene Nanocomposites Using Iron-Free Graphite[11] and Iron-Containing Graphites[a]

% KC_8	%C[b]	$T_{10\%}$ (°C)	T_{max} (°C)	char (%)
0		351	418	0
5.04	3.59	419	446	19
5.12	3.67	401	442	7
4.17	2.95	417	445	8
4.17	2.96	415	445	10
3.14	2.19	410	443	19
3.39	2.41	410	441	11
2.13	1.51	406	442	8
1.10	0.779	419	445	9
1.39	0.987	408	444	6
		Iron-Containing Graphites		
4.70	3.34	426	464	7
4.98	3.54	428	459	6
4.69	3.34	429	464	18
2.97	2.11	410	448	11
1.02	0.725	416	454	5
1.00	0.711	416	448	5
4.96	3.53	426	452	12
5.12	3.67	425	451	18
3.00	2.17	404	461	7
3.14	2.19	414	453	10
0.98	0.700	427	459	3
1.24	0.881	415	453	9

[a] %C = 0 is virgin polystyrene of 280 000 molecular weight. [b] %C is the amount of carbon from KC_8 and any extra graphite which was added to the system.

Unfortunately, it has not proved possible to obtain TEM data for these systems.

TGA of Polystyrene−Graphite Nanocomposites. There is little difference in TGA results between nitrogen and air atmospheres; the TGA results in nitrogen are shown in Table 7. The data for the iron-free graphites has been previously reported.[11] The data consists of the temperature at which 10% degradation occurs, $T_{0.1}$, the peak of the derivative of the TGA curve, T_{max}, and the fraction which is nonvolatile at 600 °C, char.

There is little, if any, difference between the iron-containing graphites and the iron-free system. It is somewhat difficult to make a direct comparison since the amount of graphite is somewhat variable, but the likely conclusion is that iron plays no role in the thermal stability of graphite nanocomposites. TGA measurements have also been carried out in air to determine if the combination of air and iron has some effect. The onset temperature of the degradation, as well as T_{max}, is unaffected by the presence of iron.

Cone Calorimetry. The cone calorimetric results are shown in Table 8; the results for the iron-free graphites have been previously reported.[11] The presence of iron in the graphite has no effect on the cone results.

In a polymer−graphite nanocomposite, the graphite is nanodispersed with the polymer but the iron, since it is an impurity, is likely to be clustered in a particular region. Thus, the iron present in graphite will have little effect in these systems since it is not as well-dispersed as in the clays.

Table 8. Cone Calorimetric Results for Iron-Free[11] and Iron-Containing Graphites

% C_8K	$t_{ignition}$[a] (s)	PHRR[a] (kW m^{-2})	t_{PHRR}[a] (s)	mean HRR[a] (kW m^{-2})	ASEA[a] (m^2 kg^{-1})	mass loss (%)	mass loss rate (mg s^{-1})
PS[6]	35	1024	165	479	1572	86.0	127
5.08	33	635	197	332	1193	80.0	107
4.17	25	670	190	352	976	82.7	114
3.26	30	665	181	352	1034	84.9	108
1.10	28	668	183	376	1009	82.5	110
PS	35	1024	165	479	1572	86	127
9092							
1%	19	746	163	381	1072	89.5	122
3%	18	620	159	352	880	84.1	106
5%	25	669	164	337	931	81.4	104
505							
1%	28	578	159	312	778	80.1	102
3%	35	703	169	332	972	81.6	109
5%	33	566	178	298	808	77.0	104

[a] $t_{ignition}$, time to ignition; PHRR, peak heat release rate; t_{PHRR}, time to peak heat release rate; mean HRR, mean heat release rate; ASEA, average specific extinction area (smoke production).

Conclusions

Polystyrene−clay nanocomposites have been prepared using different clays; the identity of the cation, rather than the type of clay, controls whether intercalation or exfoliation is observed. Intercalated structures appear to give a lower peak heat release than do exfoliated materials. Clays that contain iron show enhanced thermal stability whether measured by TGA or cone calorimetry. It then appears that structural iron is the operative site for radical trapping within the clay. On the other hand, iron appears to have no role in the thermal stability of graphite−polystyrene nanocomposites, since it is not nano-dispersed as the structural iron is in the clay.

Acknowledgment. This work was performed under the sponsorship of the U.S. Department of Commerce, National Institute of Standard and Technology, Grant No. 70NANB0H0096. The assistance of Marcel Van Den Berk and David Paul, Solutia, Inc., in obtaining the cone calorimetric data at 35 kW m^{-2} is gratefully acknowledged. The cone data at 50 kW m^{-2} was kindly provided by Michael Smith at NIST. The genesis of the idea that radical trapping may be important arose from a conversation with William H. Starnes, Jr. This work was carried out by the National Institute of Standards and Technology (NIST), an agency of the U.S. government, and all NIST data in this paper, by statute, is not subject to copyright in the United States. Certain commercial equipment, instruments, materials, or companies are identified in this paper in order to adequately specify the experimental procedure. This in no way implies endorsement or recommendation by NIST.

CM010451Y